JOURNAL OF BACTERIOLOGY, Nov. 1996, p. 6539–6545 Vol. 178, No. 22
0021-9193/96/$04.00+0
Copyright © 1996, American Society for Microbiology

# Structural Analysis of the *Leptospiraceae* and *Borrelia burgdorferi* by High-Voltage Electron Microscopy

STUART F. GOLDSTEIN,[1] KAROLYN F. BUTTLE,[2] AND NYLES W. CHARON[3]*

*Department of Genetics and Cell Biology, University of Minnesota, St. Paul, Minnesota 55108[1]; Biological Microscopy and Image Reconstruction Resource, NIH Biotechnological Resource, Wadsworth Center for Laboratories and Research, New York State Department of Health, Albany, New York 12201-0509[2]; and Department of Microbiology and Immunology, Robert C. Byrd Health Sciences Center, West Virginia University, Morgantown, West Virginia 26506-9177[3]*

Received 27 June 1996/Accepted 17 September 1996

**Spirochetes are an evolutionary and structurally unique group of bacteria. Outermost is a membrane sheath (OS), and within this sheath are the protoplasmic cell cylinder (PC) and periplasmic flagella (PFs). The PFs are attached at each end of the PC and, depending on the species, may or may not overlap in the center of the cell. The precise location of the PFs within the spirochetal cells is unknown. The PFs could lie along the cell axis. Alternatively, the PFs could wrap around the PC in either a right- or a left-handed sense. To understand the factors that cause the PFs to influence cell shape and allow the cells to swim, we determined the precise location of the PFs in the *Leptospiraceae* (*Leptonema illini*) and *Borrelia burgdorferi*. Our approach was to use high-voltage electron microscopy and analyze the three-dimensional images obtained from thick sections of embedded cells. We found that a single PF in *L. illini* is located in a central channel 29 nm in diameter running along the helix axis of the right-handed PC. The presence of the PFs is associated with the end being hook shaped. The results obtained agree with the current model of *Leptospiraceae* motility. In *B. burgdorferi*, which forms a flattened wave, the relationship between the PFs and the PC is more complicated. A multistrand ridge 67 nm in diameter, which was shown to be composed of PFs by cross-sectional and mutant analysis, was found to extend along the entire length of the cell. We found that the PFs wrapped around the PC in a right-handed sense. However, the PFs formed a left-handed helix in space. The wavelength of the cell body and the helix pitch of the PFs were found to be identical (2.83 μm). The results obtained were used to propose a model of *B. burgdorferi* motility whereby backward-propagating waves, which gyrate counterclockwise as viewed from the back of the cell, are generated by the counterclockwise rotation of the internal PFs. Concomitant with this motion, the cell is believed to rotate clockwise about the body axis as shown for the *Leptospiraceae*.**

Spirochetes are recognized for their unique cell morphology and unusual means of motility (4, 9, 31). These organisms have a protoplasmic cell cylinder (PC), which is surrounded by an outer membrane sheath (OS) (17). In the periplasm, between the peptidoglycan layer and the OS, are periplasmic flagella (PFs). Genetic evidence indicates that the PFs are necessary for motility (3, 13, 23, 24, 27, 29). Direct examination of protruding PFs has shown that the PFs rotate in a manner similar to that of flagella of other bacteria (7, 25). The PFs are inserted subterminally at each end and extend toward the opposite end. Each PF is attached at only one end (4, 17). In many spirochete species, including *Borrelia burgdorferi*, the PFs from one end of the cell are long enough to overlap in the center of the cell with those extending from the opposite end (19, 22). On the other hand, in the *Leptospiraceae*, including *Leptonema illini* (formerly *Leptospira illini*), the PFs are relatively short and do not overlap (2, 3, 18). The number of PFs attached at each end varies from species to species; in *L. illini* and other *Leptospiraceae*, it is one (2, 3); in *B. burgdorferi*, it is approximately seven (19, 22).

The *Leptospiraceae* have served as a model system for understanding spirochete motility (1, 5, 6, 9, 11, 12). These spirochetes have a right-handed cell body (a stationary right-handed helix spirals clockwise [CW], and a stationary left-handed helix spirals counterclockwise [CCW], moving away from an observer), with ends which are either hook or spiral shaped. The shape of the cell ends is determined by the structure and direction of rotation of the PFs. As viewed from the back of translating cells, rotation of the PFs in the CCW direction causes the anterior end to be spiral shaped and the posterior end to be hook shaped. Rotation of the anterior PF causes the formation of a gyrating spiral-shaped wave. This wave is sufficient to propel the cells forward in a non-gel-like liquid such as water. The right-handed cell cylinder concomitantly rolls around the PFs in the opposite direction (CW). This rolling motion allows the cell to literally screw through a gel-like medium such as 1% methylcellulose with little slippage. Nontranslating cells are often seen with both ends being either hook shaped or spiral shaped. Such cells are believed to have the PFs rotating in opposite directions.

The structure of *B. burgdorferi* is considerably more complex than that of the *Leptospiraceae*. We recently reported that, in contrast to the *Leptospiraceae* and other spirochete species (5, 8), swimming *B. burgdorferi* has a flattened wave-like shape rather than being a circular helix; this form can be approximated by circular arcs or bends connected by straight interbend regions (13). There are often axial twists, so that different regions of a cell lie in different planes. Cells frequently but briefly stop translating. These nontranslating cells are often distorted into dramatic flexes. Because a mutant that lacked PFs was characterized as being rod shaped, we concluded that an interaction between the PFs and cell cylinder dictates the

* Corresponding author. Mailing address: Department of Microbiology and Immunology, West Virginia University, Box 9177, Robert C. Byrd Health Sciences Center, Morgantown, WV 26506-9177. Phone: (304) 293-4170. Fax: (304) 293-7823. Electronic mail address: charon@wvnvms.wvnet.edu.



Downloaded from http://jb.asm.org/ on October 21, 2019 by guest

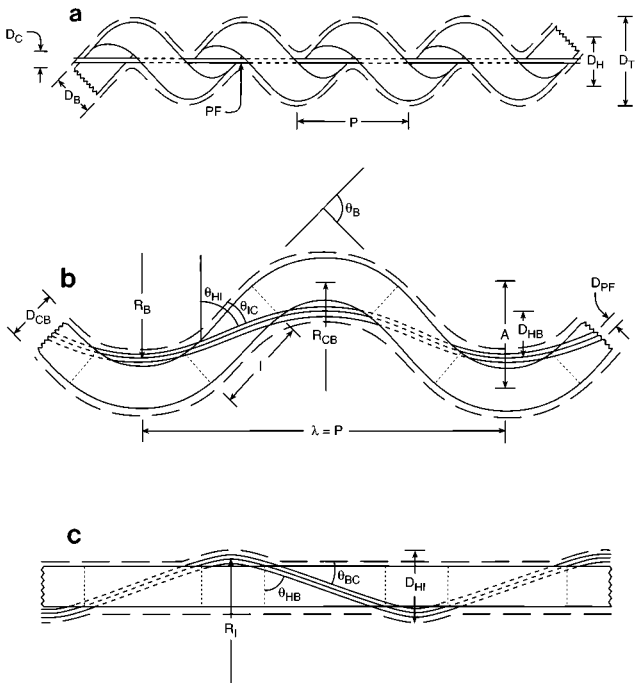


FIG. 1. Schematic representation of *L. illini* (a) and *B. burgdorferi* flat-on (b) and edge-on (c) views. Dashed lines represent the OS. Parameters are described in the text and in Table 1.

shape of the intact organism to form the flat wave (13). This interaction is evidently very complex, as purified PFs are left-handed with a defined helix diameter (0.28 μm) and pitch (1.48 μm) (7).

The motility of *B. burgdorferi* shows certain similarities to that of the *Leptospiraceae*. We observed that the backward-propagating waves on translating cells gyrated CCW (13). To generate such waves, the bundles of PFs should be left-handed and rotate in the same direction—CCW. To balance this motion, we suggested that the cell rolls CW about the body axis (13). In those cells which are flexing and are in the nontranslational mode, the bundles of PFs are believed to rotate in opposite directions.

The exact spatial relationship between the PFs and the PC has not been determined for any spirochete. In the model of translating *Leptospiraceae*, the PFs are diagrammed as running along the axis of the cell (11). However, the PFs could conceivably wrap around the PC during translation. The evidence in the literature is inconclusive, especially since many investigators analyzed distorted cells that are flattened on a grid (2, 3, 28). Some observations have been made on thin sections of embedded cells (26), but there has not been a careful examination of the position of the PFs within cells. Similarly, the spatial relationship of the PFs and the PC in *B. burgdorferi* is unclear. Hayes et al. concluded that the PFs wind in the left-handed sense in some cells and in the right-handed sense in other cells (15).

In the present study, thick sections of embedded cells of *L. illini* and *B. burgdorferi* were examined by high-voltage electron microscopy (HVEM). Our purpose was to determine the relationship of the PFs to the PC in these two spirochete species. The results obtained indicate that the PFs run along the helix axis in *L. illini* and wrap around the cells of *B. burgdorferi* in a very complicated manner. Based on these results, we now have a better understanding of the factors that dictate cell shape and also enable the cells to swim.

## MATERIALS AND METHODS

**Organisms and culture conditions.** *L. illini* 3055; *B. burgdorferi* 297, B31, and HB19; and the nonmotile PF-deficient mutant of *B. burgdorferi* isolated by Sadziene et al. have been previously described (3, 13, 29). The growth conditions and medium composition for *L. illini* and *B. burgdorferi* have been described by Bromley and Charon (3) and Goldstein et al. (13).

**Preparation of cells for electron microscopy.** To prepare *B. burgdorferi* for electron microscopy, cells were first fixed by mixing 6 ml of logarithmic-phase cells with an equal volume of 4% glutaraldehyde in 0.2 M sodium cacodylate buffer, pH 7.4 (SC buffer), and incubating for 1 h at room temperature (15). The cells were centrifuged at 745 × *g* at 4°C, and the pellet was washed with 1 to 2 ml of 0.1 M SC buffer, pH 7.4, and recentrifuged as before. After three washes, the cells were postfixed in 1% $OsO_4$ in 0.1 M SC buffer for 1.5 h at room temperature. The cells were then washed three times in 0.1 M SC buffer and stained by resuspending in 1% aqueous uranyl acetate for 30 min (16).

For embedding, the cells were centrifuged and then dehydrated through a series of acetone solutions and embedded in Epox 812 (Ernest Fullam, Latham, N.Y.). To maximize the probability that cells would lie parallel to the plane of sections, the cells were embedded between the bottom and top of plastic petri dishes. Approximately 1 to 2 ml of epoxy was placed in the inverted top of a 60-mm LUX Permanox culture dish (Lab-Tek, Naperville, Ill.), and the bottom of the dish was placed on top. It was cured for 24 h at room temperature followed by 24 h at 70°C. Cells were checked by dark-field microscopy at each stage to verify that they retained the three-dimensional shape characteristic of viable cells. These cells were compared with ones prepared by standard block embedding; no differences were detected except that the latter had shorter sections to view. Thick sections of 0.25, 0.5, and 0.75 μm were cut, mounted on Formvar-coated slot grids, and further stained with 4% aqueous uranyl acetate with 0.3% Tween solution (1:1) at 60°C for 1 h followed by lead citrate for 15 min at room temperature. Stained cells of *L. illini* were prepared by a similar procedure except that the cells were centrifuged at 12,000 × *g* for fixation and embedded by block rather than flat embedding.

**HVEM.** Electron microscopy was carried out with an AEI high-voltage electron microscope at 1.0 MV at magnifications ranging from ×8,000 to ×25,000. A colloidal gold solution (25 nm) was applied to one surface of the section for 10 min, and the excess was blotted off. The resulting particles provided a reference for orienting stereo pairs as well as negative alignment for the tilt series. Stereo pairs of negatives were taken with angular separations of 6° to 20°, depending on the specimen thickness and magnification (21). In addition, tilt series ranging

TABLE 1. Measurements and derived parameters of *L. illini* and *B. burgdorferi*[a]

| Sp. and symbol | Parameter | Value obtained |
|---|---|---|
| *L. illini* | | |
| $D_B$ | Cell body diameter | 0.147 μm |
| $D_C$ | Central channel diameter | 0.029 μm |
| $D_H$ | Cell body helix diameter | 0.176 μm |
| $D_T$ | Cell body total diameter | 0.323 μm |
| $P$ | Cell body pitch | 0.702 μm |
| *B. burgdorferi* | | |
| $A$ | Peak-to-peak amplitude | 0.78 μm |
| $D_{CB}$ | Cell body diameter | 0.33 μm |
| $D_{PF}$ | PF bundle diameter | 0.067 μm |
| $D_{HB}$ | PF bundle helix diameter, bends | 0.38 μm |
| $D_{HI}$ | PF bundle helix diameter, interbends | 0.40 μm |
| $\theta_B$ | Bend angle | 1.49 μm |
| $\theta_{IC}$ | PC-PF bundle angle, interbends | 0.37 rad |
| $\theta_{BC}$ | PC-PF bundle angle, bends | 0.45 rad |
| $\theta_{HB}$ | PF bundle pitch angle, bends | 1.12 rad |
| $\theta_{HI}$ | PF bundle pitch angle, interbends | 1.20 rad |
| $I$ | Interbend length | 0.78 μm |
| λ | Wavelength | 2.83 μm |
| $P$ | PF bundle helix pitch | 2.83 μm |
| $R_B$ | PF bundle radius of curvature, bends | 1.53 μm |
| $R_{CB}$ | Cell body bend radius | 0.83 μm |
| $R_I$ | PF bundle radius of curvature, interbends | 1.24 μm |

[a] See Fig. 1a and b for definitions.

Downloaded from http://jb.asm.org/ on October 21, 2019 by guest

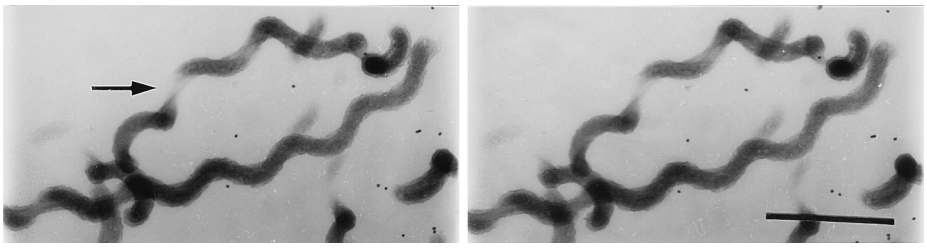

FIG. 2. HVEM image of *L. illini*. Note that the cell body is a right-handed helix. The arrow points to a PF located along the cell axis. The dark grains are gold particles added to the top surface of the sections for reference. Bar, 1.0 μm. Tilt angle = ±5°.

from +60° to −60° at 5° increments were taken of several cells, and video sequences were made for animation.

Measurements of cell dimensions (Fig. 1; Table 1) were made on prints as described previously (8). The cell body is the entire cell including the OS. We define the cell axis or helix axis as a line forming along the long axis of a cell and the body axis as a line running along the center of the PC (11). Radii of cell body bends of *B. burgdorferi* and of PF bundles within these bends were measured along their inner edge; the measurements were computer assisted (8). Datum points were spaced 0.05 μm apart. To obtain final figures for the radii of the cell body bends and PF bundles, the values of five points taken near the center of the bends were averaged and added to one-half of the cell body diameter or PF bundle width. To estimate the length of interbend regions, flat-on views of cells were used. Lines were drawn perpendicular to the cell body at the points where the PF bundle appeared to cross the edges of the cell body. Computer-assisted measurements of the distance between pairs of lines were made along both edges of the cell body in an interbend region, and their average value was taken as the length of that interbend region. The helix diameter of the cell body of *L. illini* was calculated as the total width of the cell ($D_T$) minus the cell body diameter ($D_B$). The peak-to-peak-amplitude ($A$) of the cell body of *B. burgdorferi* was calculated as the total amplitude of the cell body minus the cell body diameter ($D_{CB}$). The diameter of the central channel of *L. illini* was calculated as the total width ($D_T$) minus $2 \times D_B$.

## RESULTS

**Analysis of *L. illini*.** We analyzed the structure of spirochetes with stereo pairs of thick sections. Dark-field microscopy of fixed *L. illini* revealed that the cells resembled viable cells except that both ends were always hook shaped; none of the ends were spiral shaped. These results are consistent with previous observations that cells at rest have exclusively hook-shaped ends (1, 3). As previously noted (5), *L. illini* had a right-handed cell body (Fig. 2). The helix pitch ($P$) was 0.702 ± 0.043 μm ($n$ = 17 cells; see Fig. 1a and Table 1 for description and values of parameters), which agrees well with the value of 0.69 ± 0.04 μm measured on live cells (13). The diameter ($D_B$) of the cell body was 0.147 ± 0.012 μm, and the total width ($D_T$) of the cell bodies was 0.323 ± 0.024 μm ($n$ = 17 cells). The helix diameter ($D_H$) of the cell body was calculated to be 0.176 μm. A central channel in the region of the helix axis with a calculated diameter ($D_C$) of 0.029 μm ran along the length of the spirochete. A single PF was located within the central channel, and that region of the cell was hook shaped. In none of the cells observed did the PF wrap around the cell cylinder.

**General features of wild-type *B. burgdorferi*.** As observed by dark-field microscopy, fixed wild-type cells of *B. burgdorferi* B31, 297, and HB19 resembled swimming cells; these cells had flattened waveforms and axial twists (Fig. 3 to 7). We found that lower magnifications (×8,000 to ×12,000) were most useful for visualizing the geometry of the cells in relation to the PFs. Specifically, low magnification best allowed us to determine whether the PFs were above or below the PC or extended along the cell axis. In addition, some fixed cells appeared which resembled cells that were flexing at the time of fixation, as they appeared irregular and twisted. In general, there was more variability with respect to cell forms in fixed cells compared with swimming cells.

Measurements reported here were made on those cells whose shapes appeared qualitatively similar to the swimming form of live cells. Helicity could be discerned in some cells, but for the most part even these cells were flattened rather than forming circular helices. The OS was not readily distinguishable except in an occasional cross section. A noticeable ridge wound around the length of all cells. This ridge had a diameter of 67 ± 11 nm ($n$ = 9 cells). In both longitudinal sections and cross sections, the ridge appeared as a bundle of multistranded filamentous structures resembling PFs (Fig. 3 and 4a).

**Structural details of cell bodies of *B. burgdorferi* B31 and 297.** Measurements were made of cells in electron micrographs (Table 1 and Fig. 1b and c) and compared with those previously obtained from photographs of live cells taken by light microscopy (13). We compared the diameter of the cell body in the regions within bends with those with the interbend regions

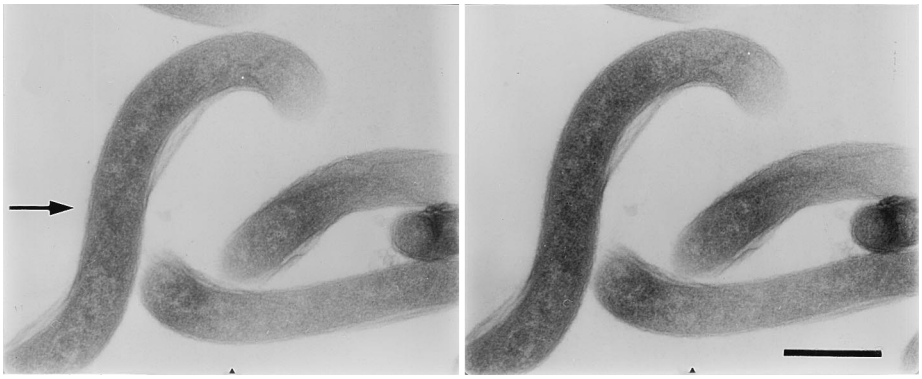

FIG. 3. HVEM image of *B. burgdorferi* B31. Arrow points to a region of the cell where the filamentous ridge crosses over the top of the cell from lower left to upper right. Bar, 0.5 μm. Tilt angle = ±3°.

Downloaded from http://jb.asm.org/ on October 21, 2019 by guest

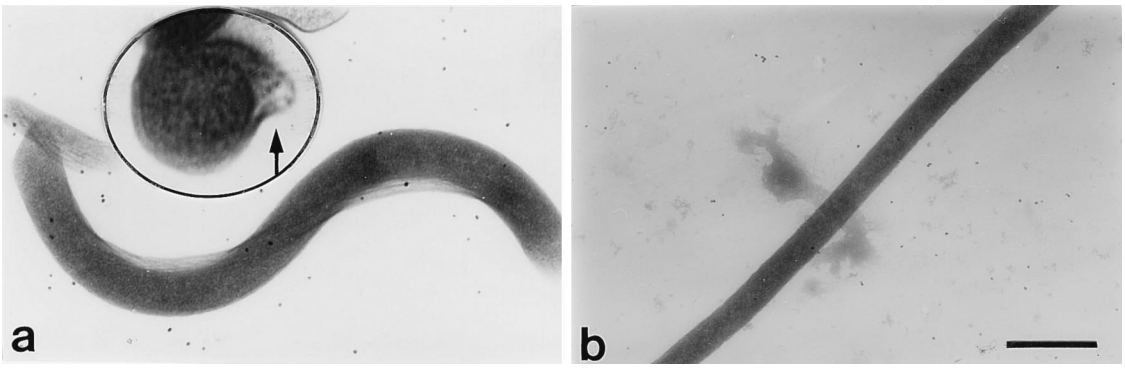


FIG. 4. HVEM images of *B. burgdorferi* HB19 wild type (a) and PF-deficient mutant (b). The inset is a cross-section showing the filamentous nature of the ridge (arrow). Six filaments were discernable in the photographic negatives. Note that wild-type strain HB19 resembled strain 297 (Fig. 3) and that the PF mutant lacked the ridge and was rod shaped. (a) Bar, 0.6 μm (inset, 0.2 μm); (b) bar, 0.96 μm.

in face-on views. No difference in diameter ($D_{CB}$) was distinguishable (0.34 ± 0.02 μm [$n$ = 42 interbend regions on 20 cells] versus 0.33 ± 0.02 μm [$n$ = 26 bends on 20 cells]). The radius ($R_{CB}$) of cell body bends was 0.83 ± 0.23 μm ($n$ = 17 bends on nine cells), which agrees well with the value of 0.72 ± 0.11 μm measured on live cells (13). The wavelength (λ) of the cell bodies was 2.83 ± 0.34 μm ($n$ = 22 cells), which agrees reasonably well with the value of 3.19 ± 0.34 μm measured on live cells (13). The length ($I$) of the interbend regions was 0.78 ± 0.10 μm ($n$ = 16 regions on nine cells), which resembled that calculated from measurements on live cells (0.79 μm [13]). Considering the differences in methods of measurement of the interbend regions, these figures agree surprisingly well. The peak-to-peak amplitude ($A$) was 0.78 ± 0.08 μm ($n$ = 11 sets of bends on seven cells). The angle ($\theta_B$) subtended by the bends was 1.49 ± 0.28 rad ($n$ = 12 bends on seven cells). Because the cells were generally somewhat oblique to the plane of the section, these last two figures are probably slightly smaller than the actual values. These values are in good agreement with the values of 0.85 ± 0.20 μm and 1.54 ± 0.23 rad, respectively, measured on live cells.

**Analysis of a PF-deficient mutant.** We compared the structure of the wild-type *B. burgdorferi* with a mutant that lacked PFs. Sadziene et al. isolated a spontaneously occurring nonmotile mutant of *B. burgdorferi* HB19 that lacked PFs (29). Light microscopy of viable cells of the PF-deficient mutant previously indicated that it was rod shaped, as it lacked both helicity and the wave-like character of the wild type (13). To test whether the ridge running along the cell body actually contained a bundle of PFs, we analyzed the structure of the PF-deficient mutant and compared it with wild-type HB19. Whereas wild-type cells of HB19 were wave-like and had a ridge running along their cell cylinder (Fig. 4a), the mutant cells were straight (Fig. 4b) (13) with a diameter ($D_{CB}$) of 0.32 ± 0.03 μm ($n$ = 21 cells). This diameter is similar to that of wild-type cells (Fig. 4a). No ridge was detected in any of the PF-deficient mutant cells. These results, along with the cross-sectional analysis (inset, Fig. 4a), further support our assertion that the ridge is composed of a bundle of PFs. In addition, as observed with live cells (13), mutant cells tended to wrap around one another in a right-handed sense (not shown).

**Analysis of PF bundles on strains B31 and 297.** As noted above, the PFs were found to group into a single ridge or bundle that extended from one end of the cell to the other.

FIG. 5. HVEM image of *B. burgdorferi* 297 in an oblique orientation. Arrows point to regions of the cell where the ridge crosses over the top of the cell from lower left to upper right. The dark grains are gold particles located on the top surface of the section. Bar, 1.0 μm. Tilt angle = ±5°.

Downloaded from http://jb.asm.org/ on October 21, 2019 by guest

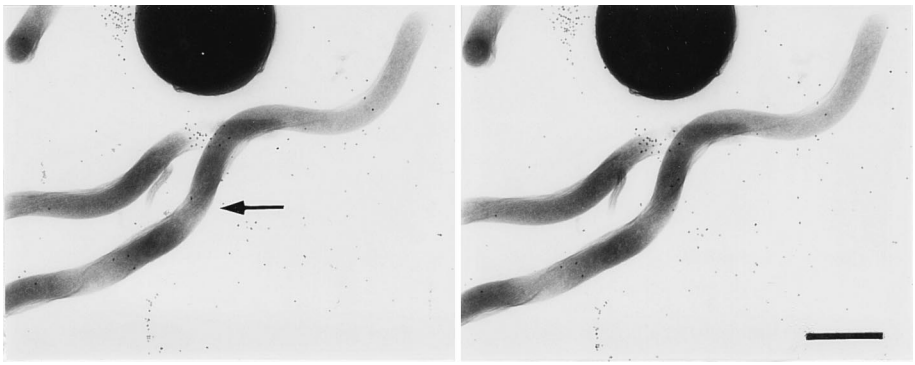

FIG. 6. HVEM image of *B. burgdorferi* 297 with axial twist. Bottom of cell is edge-on, and top is face-on. Arrow points to regions as described for Fig. 5. The dark grains are gold particles located on the top surface of the section. Bar, 1.0 μm. Tilt angle = ±6°.

Occasionally, the bundle split into two separate bundles (not shown). Previous studies have indicated that the PFs overlap in the center of the cell and form a bundle (19), but this overlapping region could not be distinguished in our analysis. The results indicate that the overlapping PFs in effect form a single structural bundle that extends along the length of the cell.

Stereo pair analysis indicated that the PF bundle formed a helix as it wound around the PC. Analysis of flat-on views and some oblique views of cells (Fig. 5) indicated that, within the bends of the PC, the PF bundle was always on the axial (inner) side of the PC ($n$ = 48 bends on 24 cells). PFs were also on the axial side of bends within axial twists (Fig. 6). In edge-on views, it was usually difficult to determine whether the PF bundle was above or below the plane of the PC and whether the PF bundle was on the axial side of the PC. However, occasionally edge-on views of cells were obtained in which the top of the bend was sliced off during sectioning. In such photographs, the PC was always sliced off and the PF bundle remained ($n$ = 8) (Fig. 7). These results further indicate that the PFs were located on the axial side of the bend.

The PF bundle always wound around the PC (i.e., body axis) in a right-handed sense (Fig. 3 and 5 to 7). The handedness was determined by noting that a vertical right-handed helix passes from lower left to upper right on the side nearest to the viewer and from lower right to upper left on the opposite side. On some cells, it was not possible to tell from direct visual impressions whether a PF bundle was in front of or behind the PC. However, in edge-on and some oblique views, it was generally easy to see whether a bend of the PC projected upward toward the viewer or downward, away from the viewer. Knowing that the PF bundle lay on the axial side of the PC in bends allowed unambiguous identification of the near and far sides of a PF bundle. The radius ($R_B$) of the PF bundles in these bends, as measured in flat-on views of cells, was 1.53 ± 0.57 μm (17 bends, nine cells). However, this parameter was difficult to measure accurately and should be taken as only approximate. The angle ($\theta_{BC}$) between the PF bundle and the cell axis within bends, as measured in edge-on views of cells, was 0.45 ± 0.05 rad ($n$ = 13 bends on seven cells). The angle ($\theta_{IC}$) between the PF bundle and the body axis in interbend regions, as determined by flat-on views of cells, was 0.37 ± 0.04 rad ($n$ = 16 regions on nine cells).

Although the PFs wound around the PC in a right-handed sense, they formed a left-handed helix in space, i.e., they formed a left-handed helix about the cell axis ($n$ = 38 cells). This left-handed form is a consequence of the wrapping of the

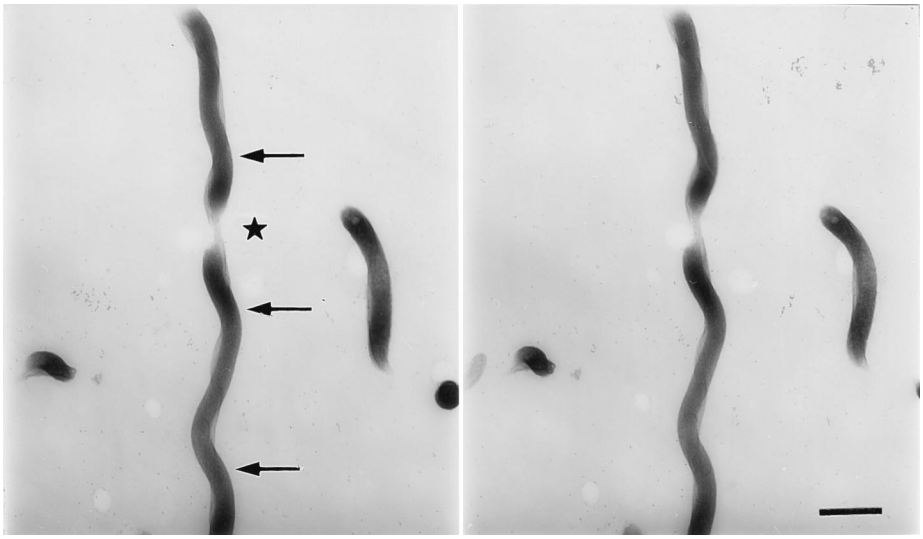

FIG. 7. HVEM image of *B. burgdorferi* 297 with an axial twist. Bottom part of cell is flat-on, and top part of cell is face-on. The star identifies an uppermost sector of the cell that was cut off during sectioning, revealing that the ridge runs underneath. Arrows point to regions as described for Fig. 5. Bar, 1.0 μm. Tilt angle = ±10°.

Downloaded from http://jb.asm.org/ on October 21, 2019 by guest

PFs around the PC in a right-handed sense with the PC being a flat wave (Fig. 1b and c). Specifically, in edge-on views, the far side of a PF helix lay between the PC and the viewer; the near side of the PF helix lay behind the PC (Fig. 1b and c). The pitch ($P$) of the PF helix was the same as the wavelength ($\lambda$) of the cell body (2.83 ± 0.34 μm [$n$ = 22 cells]).

## DISCUSSION

In this analysis, HVEM was used to analyze the relationship of the PFs and the cell cylinders of two species of spirochetes. We first attempted a similar structural analysis by serial sectioning (14). However, we found that locating a given cell in a set of serial sections and accurately determining its chirality were difficult. In addition, because serial sections are not infinitely thin, the thickness of the section limited the resolution of the reconstructed image. In contrast, HVEM of thick sections allowed us to view the entire width of a cell in a single electron micrograph. Such specimens were easy to control for image reversal. With stereo pair analysis, HVEM permitted us to obtain high-resolution three-dimensional images with considerable depth.

The general form seen of *L. illini* cells agrees with previous reports concerning cell shapes and dimensions. As expected, these spirochetes had a readily discernable right-handed cell body with a single PF near the cell ends. Measurements of the helix pitch agree well with measurements on live cells (12). Reliable figures for some dimensions could not be obtained from light micrographs. Because only hook-shaped ends were seen in fixed cells, the form of the anterior spiral-shaped end could not be determined in this study. The cell body diameter ($D_B$) (0.147 μm) measured in this study is similar to the results found by others (20, 26). The helix diameter ($D_H$) of the cell body was 0.176 μm. This figure is noticeably smaller than the figure of 0.24 ± 0.05 μm obtained from light micrographs (12). As previously noted, the helix diameter is very hard to calculate accurately from measurements on light micrographs. The figure reported here is probably a more reliable estimate.

Because we found that the PFs run down the helix axis of the cell, we now have a better understanding of how the *Leptospiraceae* swim. The results indicate that rotation of the more rigid PFs causes the cells to gyrate in the manner first diagrammed by Berg et al. and later modified by Goldstein and Charon (1, 11). Evidently, there is no wrapping of the PFs around the PC. Although we could not discern the spiral-shaped ends in our analysis, we consider it unlikely that the PFs wrap around the PC at these ends. Switching from a hook-shaped end to a spiral-shaped end occurs quite readily. Having the PFs lie along the helix axis in both forms should be mechanically more efficient than having one form with the PF lying along the helix axis and the other wrapping around the PC. The diameter ($D_C$) of the channel through which the PFs run was determined to be 0.029 μm. Because the diameter of the PFs has been measured to be between 0.012 and 0.025 μm (18, 26, 28, 30), the fit of the PF with the cell cylinder is obviously quite tight.

*B. burgdorferi* fixed cells in the present study looked similar to live cells viewed with light microscopy (13). However, the shapes of the fixed cells appeared to be somewhat more variable than those of live ones. The PF-deficient mutant of HB19 appeared rod shaped, in agreement with light microscopic observations (13). The cell body diameter of mutant cells ($D_{CB}$) was similar to that of wild-type cells. Clusters of the PF-deficient mutants had curved cell bodies (10), suggesting that these organisms are quite flexible.

Flat waves travel along the cell body of swimming *B. burgdorferi*. These waves are thought to be moved along the cell by rotating left-handed helical PF bundles (13). In the present study, the PFs were found to have a left-handed helical shape within the cell, as predicted by this model. The shape of the PF helix can be determined from the measurements made on the photographs. The radius of curvature of the PF helix within interbend regions $\{(R_I) = D_{CB}/[(2)\sin^2\theta_{IC}] = 1.24$ μm$\}$ was similar to its radius of curvature within the bends ($R_B$ = 1.53 μm). The helix diameter in face-on views was similar to that in edge-on views: the helix diameter in face-on views ($D_{HB}$) = $A - D_{PF} - D_{CB}$ = 0.38 μm; the helix diameter in edge-on views ($D_{HI}$) = $D_{PF} + D_{CB}$ = 0.40 μm. The pitch angle in bends ($\theta_{HB}$) as seen in edge-on views = $\pi/2 - \theta_{BC}$ = 1.12 rad. The pitch angle in interbends ($\theta_{HI}$) seen in face-on views = $(\pi - \theta_B)/2 + \theta_{IC}$ = 1.20 rad. These calculations indicate that the PF helix is circular and that the radius of curvature and pitch angle within bends were similar to those within interbends. The form of the PF helix in the transition between bends and interbends was not studied in detail. The PF bundle could possibly deviate from being helical in this transition region. Note that purified PFs are left-handed and have a different helix pitch (1.48 μm) and helix diameter (0.28 μm) (7) from the PF bundle observed in situ (helix pitch [$P$] = 2.83 μm, helix diameter [$D_{HB}$, $D_{HI}$] = 0.40 μm). These results suggest that torsional forces of the PFs and cell cylinder influence PF bundle shape in a very complicated way.

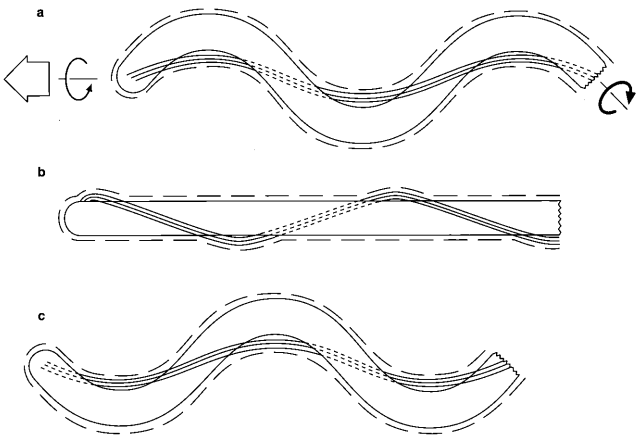


FIG. 8. Configurations of PFs and PC of *B. burgdorferi* cell moving toward the left of the figure (open arrow). The OS is represented by a dashed line. The cell forms a flat wave. In the proposed model, the cell rolls CCW (thin arrow) as the PFs rotate CCW as viewed from behind the cell. The waves concomitantly move toward the back of the cell and generate forward thrust. To balance the torque generated by this motion, the cell rotates around the body axis CW (thick arrow). The cell is drawn rotating CCW at 0°, face-on (a); 90°, edge-on (b); and 180°, face-on (c).

Although the PFs have a left-handed helical shape, they wrap around the PC axis in a right-handed sense with one turn per wavelength. This result is not unexpected: if a flexible rod is wrapped around a left-handed helix in the right-handed sense with one winding per pitch of the helix, it forms a flat wave similar to the shape of *B. burgdorferi*; if it is wrapped around the helix in the left-handed sense, it simply ends up running down the axis of the helix. Pairs of PF-deficient mutant cells often wind around one another; they consistently wind in the right-handed sense (10, 13), suggesting that the PC may be designed to wrap around the PF bundle in the right-handed sense.

A model of *B. burgdorferi* motility is diagrammed in Fig. 8. We have previously shown that, as a translating cell swims,

Downloaded from http://jb.asm.org/ on October 21, 2019 by guest

backward-propagating flat waves generate the force needed for forward movement. In addition, these waves gyrate CCW (13). As shown in the diagram, these waves are thought to be generated by CCW rotation of the left-handed PF bundles. Cells beat at 5 to 10 Hz in growth medium at room temperature (13). Because the helix pitch of the PFs (*P*) in situ is identical to the wavelength of the cell body (λ), evidently the PF bundles rotate at this same rate. To balance the torque generated by this motion, we suggest that the cell rolls CW about the body axis as the cell swims forward.

The helical PF bundle and the rod-shaped PC of *B. burgdorferi* wrap around one another and distort each other to produce a flat, meandering waveform. This shape is very stable, as it is seen in both translating and nontranslating cells. In addition, this shape forms quickly when flexed cells resume translation. How *B. burgdorferi* balances the forces between its PFs and PC to produce this flat shape, even when the PFs are rotating within it, remains an intriguing question. Comparisons of the results reported here with similar studies on other spirochete species should yield a better overall understanding concerning the complex geometry and motility of this unique group of bacteria.

## ACKNOWLEDGMENTS

We thank R. C. Johnson for his encouragement and assistance, T. Harper for the early serial-section analysis, and D. DeRosier for suggestions. We also thank T. Beveridge for first suggesting HVEM as an approach to analyze PF structure in situ and R. Kuehn for flat embedment methodology.

This research was supported by grant numbers AI29743, DE04645, and DE012046 from the United States Public Health Service. In addition, K.F.B. and the HVEM facility were supported by grant number RR 01219 awarded by the Biotechnology Area, National Center for Research Resources (DHHR/PHS), to support the Wadsworth Center's Biological Microscopy and Image Reconstruction Facility as a National Biotechnological Resource.

## REFERENCES

1. **Berg, H. C., D. B. Bromley, and N. W. Charon.** 1978. Leptospiral motility. Symp. Soc. Gen. Microbiol. **28:**285–294.
2. **Birch-Andersen, A., K. Hovind-Hougen, and C. Borg-Petersen.** 1973. Electron microscopy of *Leptospira*. 1. *Leptospira* strain Pomona. Acta Pathol. Microbiol. Scand. Sect. B **81:**665–676.
3. **Bromley, D. B., and N. W. Charon.** 1979. Axial filament involvement in the motility of *Leptospira interrogans*. J. Bacteriol. **137:**1406–1412.
4. **Canale-Parola, E.** 1984. The spirochetes, p. 38–70. *In* N. R. Krieg and J. G. Holt (ed.), Bergey's manual of systematic bacteriology. Williams and Wilkins, Baltimore.
5. **Carleton, O., N. W. Charon, P. Allender, and S. O'Brien.** 1979. Helix handedness of *Leptospira interrogans* as determined by scanning electron microscopy. J. Bacteriol. **137:**1413–1416.
6. **Charon, N. W., G. R. Daughtry, R. S. McCluskey, and G. N. Franz.** 1984. Microcinematographic analysis of tethered *Leptospira illini*. J. Bacteriol. **160:** 1067–1073.
7. **Charon, N. W., S. F. Goldstein, S. M. Block, K. Curci, J. D. Ruby, J. A. Kreiling, and R. J. Limberger.** 1992. Morphology and dynamics of protruding spirochete periplasmic flagella. J. Bacteriol. **174:**832–840.
8. **Charon, N. W., S. F. Goldstein, K. Curci, and R. J. Limberger.** 1991. The bent-end morphology of *Treponema phagedenis* is associated with short, left-handed periplasmic flagella. J. Bacteriol. **173:**4820–4826.
9. **Charon, N. W., E. P. Greenberg, M. B. H. Koopman, and R. J. Limberger.** 1992. Spirochete chemotaxis, motility, and the structure of the spirochetal periplasmic flagella. Res. Microbiol. **143:**597–603.
10. **Goldstein, S. F., K. F. Buttle, and N. W. Charon.** 1996. Unpublished data.
11. **Goldstein, S. F., and N. W. Charon.** 1988. The motility of the spirochete *Leptospira*. Cell Motil. Cytoskeleton **9:**101–110.
12. **Goldstein, S. F., and N. W. Charon.** 1990. Multiple exposure photographic analysis of a motile spirochete. Proc. Natl. Acad. Sci. USA **87:**4895–4899.
13. **Goldstein, S. F., N. W. Charon, and J. A. Kreiling.** 1994. *Borrelia burgdorferi* swims with a planar waveform similar to that of eukaryotic flagella. Proc. Natl. Acad. Sci. USA **91:**3433–3437.
14. **Harper, T., and N. W. Charon.** 1996. Unpublished data.
15. **Hayes, S. F., W. Burgdorfer, and A. G. Barbour.** 1983. Bacteriophage in the *Ixodes dammini* spirochete, etiological agent of Lyme disease. J. Bacteriol. **154:**1436–1439.
16. **Hechemy, K. E., W. A. Samsonoff, H. L. Harris, and M. McKee.** 1992. Adherence and entry of *Borrelia burgdorferi* in Vero cells. J. Med. Microbiol. **36:**229–238.
17. **Holt, S. C.** 1978. Anatomy and chemistry of spirochetes. Microbiol. Rev. **42:**114–160.
18. **Hovind Hougen, K.** 1979. Leptospiraceae: a new family to include *Leptospira* Noguchi 1917 and *Leptospira* gen. nov. Int. J. Syst. Bacteriol. **29:**245–251.
19. **Hovind Hougen, K.** 1984. Ultrastructure of spirochetes isolated from *Ixodes ricinus* and *Ixodes dammini*. Yale J. Biol. Med. **57:**543–548.
20. **Hovind-Hougen, K., M. Cinco, G. M. Roomans, and A. Birch-Andersen.** 1981. Electron microscopy and X-ray microanalysis of a halophilic leptospire. Arch. Microbiol. **130:**339–343.
21. **Hudson, B., and M. J. Makin.** 1970. The optimum tilt angle for electron stereo-microscopy. J. Sci. Instrum. **3:**311.
22. **Johnson, R. C., F. W. Schmid, F. W. Hyde, A. G. Steigerwalt, and D. J. Brenner.** 1984. *Borrelia burgdorferi* sp. nov.: etiological agent of Lyme disease. Int. J. Syst. Bacteriol. **34:**596–597.
23. **Li, H., J. Ruby, N. Charon, and H. Kuramitsu.** 1996. Gene inactivation in the oral spirochete *Treponema denticola*: construction of a *flgE* mutant. J. Bacteriol. **178:**3664–3667.
24. **Limberger, R. J., and N. W. Charon.** 1986. *Treponema phagedenis* has at least two proteins residing together on its periplasmic flagella. J. Bacteriol. **166:** 105–112.
25. **Macnab, R. M.** 1992. Genetics and biogenesis of bacterial flagella. Annu. Rev. Genet. **26:**131–158.
26. **Nauman, R. K., S. C. Holt, and C. D. Cox.** 1969. Purification, ultrastructure, and composition of axial filaments from *Leptospira*. J. Bacteriol. **98:**264–280.
27. **Paster, B. J., and E. Canale-Parola.** 1980. Involvement of periplasmic fibrils in motility of spirochetes. J. Bacteriol. **141:**359–364.
28. **Ritchie, A. E., and H. C. Ellinghausen.** 1965. Electron microscopy of leptospires. I. Anatomical features of *Leptospira pomona*. J. Bacteriol. **89:**223–233.
29. **Sadziene, A., D. D. Thomas, V. G. Bundoc, S. C. Holt, and A. G. Barbour.** 1991. A flagella-less mutant of *Borrelia burgdorferi*. Structural, molecular, and in vitro characterization. J. Clin. Invest. **88:**82–92.
30. **Trueba, G. A., C. A. Bolin, and R. L. Zuerner.** 1992. Characterization of the periplasmic flagellum proteins of *Leptospira interrogans*. J. Bacteriol. **174:** 4761–4768.
31. **Woese, C. R.** 1987. Bacterial evolution. Microbiol. Rev. **51:**221–271.

Downloaded from http://jb.asm.org/ on October 21, 2019 by guest